Observation of Electromagnetic Dalitz decays $J/\psi \to Pe^+e^-$

M. Ablikim[1], M. N. Achasov[8,a], X. C. Ai[1], O. Albayrak[4], M. Albrecht[3], D. J. Ambrose[41], F. F. An[1], Q. An[42], J. Z. Bai[1], R. Baldini Ferroli[19A], Y. Ban[28], J. V. Bennett[18], M. Bertani[19A], J. M. Bian[40], E. Boger[21,b], O. Bondarenko[22], I. Boyko[21], S. Braun[37], R. A. Briere[4], H. Cai[47], X. Cai[1], O. Cakir[36A], A. Calcaterra[19A], G. F. Cao[1], S. A. Cetin[36B], J. F. Chang[1], G. Chelkov[21,b], G. Chen[1], H. S. Chen[1], J. C. Chen[1], M. L. Chen[1], S. J. Chen[26], X. Chen[1], X. R. Chen[23], Y. B. Chen[1], H. P. Cheng[16], X. K. Chu[28], Y. P. Chu[1], D. Cronin-Hennessy[40], H. L. Dai[1], J. P. Dai[1], D. Dedovich[21], Z. Y. Deng[1], A. Denig[20], I. Denysenko[21], M. Destefanis[45A,45C], W. M. Ding[30], Y. Ding[24], C. Dong[27], J. Dong[1], L. Y. Dong[1], M. Y. Dong[1], S. X. Du[49], J. Z. Fan[35], J. Fang[1], S. S. Fang[1], Y. Fang[1], L. Fava[45B,45C], C. Q. Feng[42], C. D. Fu[1], J. L. Fu[26], O. Fuks[21,b], Q. Gao[1], Y. Gao[35], C. Geng[42], K. Goetzen[9], W. X. Gong[1], W. Gradl[20], M. Greco[45A,45C], M. H. Gu[1], Y. T. Gu[11], Y. H. Guan[1], A. Q. Guo[27], L. B. Guo[25], T. Guo[25], Y. P. Guo[20], Y. L. Han[1], F. A. Harris[39], K. L. He[1], M. He[1], Z. Y. He[27], T. Held[3], Y. K. Heng[1], Z. L. Hou[1], C. Hu[25], H. M. Hu[1], J. F. Hu[37], T. Hu[1], G. M. Huang[5], G. S. Huang[42], H. P. Huang[47], J. S. Huang[14], L. Huang[1], X. T. Huang[30], Y. Huang[26], T. Hussain[44], C. S. Ji[42], Q. Ji[1], Q. P. Ji[27], X. B. Ji[1], X. L. Ji[1], L. L. Jiang[1], L. W. Jiang[47], X. S. Jiang[1], J. B. Jiao[30], Z. Jiao[16], D. P. Jin[1], S. Jin[1], T. Johansson[46], N. Kalantar-Nayestanaki[22], X. L. Kang[1], X. S. Kang[27], M. Kavatsyuk[22], B. Kloss[20], B. Kopf[3], M. Kornicer[39], W. Kuehn[37], A. Kupsc[46], W. Lai[1], J. S. Lange[37], M. Lara[18], P. Larin[13], M. Leyhe[3], C. H. Li[1], Cheng Li[42], Cui Li[42], D. Li[17], D. M. Li[49], F. Li[1], G. Li[1], H. B. Li[1], J. C. Li[1], K. Li[30], K. Li[12], Lei Li[1], P. R. Li[38], Q. J. Li[1], T. Li[30], W. D. Li[1], W. G. Li[1], X. L. Li[30], X. N. Li[1], X. Q. Li[27], Z. B. Li[34], H. Liang[42], Y. F. Liang[32], Y. T. Liang[37], D. X. Lin[13], B. J. Liu[1], C. L. Liu[4], C. X. Liu[1], F. H. Liu[31], Fang Liu[1], Feng Liu[5], H. B. Liu[11], H. H. Liu[15], H. M. Liu[1], J. Liu[1], J. P. Liu[47], K. Liu[35], K. Y. Liu[24], P. L. Liu[30], Q. Liu[38], S. B. Liu[42], X. Liu[23], Y. B. Liu[27], Z. A. Liu[1], Zhiqiang Liu[1], Zhiqing Liu[20], H. Loehner[22], X. C. Lou[1,c], G. R. Lu[14], H. J. Lu[16], H. L. Lu[1], J. G. Lu[1], X. R. Lu[38], Y. Lu[1], Y. P. Lu[1], C. L. Luo[25], M. X. Luo[48], T. Luo[39], X. L. Luo[1], M. Lv[1], F. C. Ma[24], H. L. Ma[1], Q. M. Ma[1], S. Ma[1], T. Ma[1], X. Y. Ma[1], F. E. Maas[13], M. Maggiora[45A,45C], Q. A. Malik[44], Y. J. Mao[28], Z. P. Mao[1], J. G. Messchendorp[22], J. Min[1], T. J. Min[1], R. E. Mitchell[18], X. H. Mo[1], Y. J. Mo[5], H. Moeini[22], C. Morales Morales[13], K. Moriya[18], N. Yu. Muchnoi[8,a], H. Muramatsu[40], Y. Nefedov[21], I. B. Nikolaev[8,a], Z. Ning[1], S. Nisar[7], X. Y. Niu[1], S. L. Olsen[29], Q. Ouyang[1], S. Pacetti[19B], M. Pelizaeus[3], H. P. Peng[42], K. Peters[9], J. L. Ping[25], R. G. Ping[1], R. Poling[40], N. Q.[47], M. Qi[26], S. Qian[1], C. F. Qiao[38], L. Q. Qin[30], X. S. Qin[1], Y. Qin[28], Z. H. Qin[1], J. F. Qiu[1], K. H. Rashid[44], C. F. Redmer[20], M. Ripka[20], G. Rong[1], X. D. Ruan[11], A. Sarantsev[21,d], K. Schoenning[46], S. Schumann[20], W. Shan[28], M. Shao[42], C. P. Shen[2], X. Y. Shen[1], H. Y. Sheng[1], M. R. Shepherd[18], W. M. Song[1], X. Y. Song[1], S. Spataro[45A,45C], B. Spruck[37], G. X. Sun[1], J. F. Sun[14], S. S. Sun[1], Y. J. Sun[42], Y. Z. Sun[1], Z. J. Sun[1], Z. T. Sun[42], C. J. Tang[32], X. Tang[1], I. Tapan[36C], E. H. Thorndike[41], D. Toth[40], M. Ullrich[37], I. Uman[36B], G. S. Varner[39], B. Wang[27], D. Wang[28], D. Y. Wang[28], K. Wang[1], L. L. Wang[1], L. S. Wang[1], M. Wang[30], P. Wang[1], P. L. Wang[1], Q. J. Wang[1], S. G. Wang[28], W. Wang[1], X. F. Wang[35], Y. D. Wang[19A], Y. F. Wang[1], Y. Q. Wang[20], Z. Wang[1], Z. G. Wang[1], Z. H. Wang[42], Z. Y. Wang[1], D. H. Wei[10], J. B. Wei[28], P. Weidenkaff[20], S. P. Wen[1], M. Werner[37], U. Wiedner[3], M. Wolke[46], L. H. Wu[1], N. Wu[1], Z. Wu[1], L. G. Xia[35], Y. Xia[17], D. Xiao[1], Z. J. Xiao[25], Y. G. Xie[1], Q. L. Xiu[1], G. F. Xu[1], L. Xu[1], Q. J. Xu[12], Q. N. Xu[38], X. P. Xu[33], Z. Xue[1], L. Yan[42], W. B. Yan[42], W. C. Yan[42], Y. H. Yan[17], H. X. Yang[1], L. Yang[47], Y. Yang[5], Y. X. Yang[10], H. Ye[1], M. Ye[1], M. H. Ye[6], B. X. Yu[1], C. X. Yu[27], H. W. Yu[28], J. S. Yu[23], S. P. Yu[30], C. Z. Yuan[1], W. L. Yuan[26], Y. Yuan[1], A. Yuncu[36B], A. A. Zafar[44], A. Zallo[19A], S. L. Zang[26], Y. Zeng[17], B. X. Zhang[1], B. Y. Zhang[1], C. Zhang[26], C. B. Zhang[17], C. C. Zhang[1], D. H. Zhang[1], H. H. Zhang[34], H. Y. Zhang[1], J. J. Zhang[1], J. Q. Zhang[1], J. W. Zhang[1], J. Y. Zhang[1], J. Z. Zhang[1], S. H. Zhang[1], X. J. Zhang[1], X. Y. Zhang[30], Y. Zhang[1], Y. H. Zhang[1], Z. H. Zhang[5], Z. P. Zhang[42], Z. Y. Zhang[47], G. Zhao[1], J. W. Zhao[1], Lei Zhao[42], Ling Zhao[1], M. G. Zhao[27], Q. Zhao[1], Q. W. Zhao[1], S. J. Zhao[49], T. C. Zhao[1], X. H. Zhao[26], Y. B. Zhao[1], Z. G. Zhao[42], A. Zhemchugov[21,b], B. Zheng[43], J. P. Zheng[1], Y. H. Zheng[38], B. Zhong[25], L. Zhou[1], Li Zhou[27], X. Zhou[47], X. K. Zhou[38], X. R. Zhou[42], X. Y. Zhou[1], K. Zhu[1], K. J. Zhu[1], S. H. Zhu[1], X. L. Zhu[35], Y. C. Zhu[42], Y. S. Zhu[1], Z. A. Zhu[1], J. Zhuang[1], B. S. Zou[1], J. H. Zou[1]

(BESIII Collaboration)

[1] *Institute of High Energy Physics, Beijing 100049, People's Republic of China*
[2] *Beihang University, Beijing 100191, People's Republic of China*
[3] *Bochum Ruhr-University, D-44780 Bochum, Germany*
[4] *Carnegie Mellon University, Pittsburgh, Pennsylvania 15213, USA*
[5] *Central China Normal University, Wuhan 430079, People's Republic of China*
[6] *China Center of Advanced Science and Technology, Beijing 100190, People's Republic of China*
[7] *COMSATS Institute of Information Technology, Lahore, Defence Road, Off Raiwind Road, 54000 Lahore*
[8] *G.I. Budker Institute of Nuclear Physics SB RAS (BINP), Novosibirsk 630090, Russia*
[9] *GSI Helmholtzcentre for Heavy Ion Research GmbH, D-64291 Darmstadt, Germany*
[10] *Guangxi Normal University, Guilin 541004, People's Republic of China*
[11] *GuangXi University, Nanning 530004, People's Republic of China*
[12] *Hangzhou Normal University, Hangzhou 310036, People's Republic of China*
[13] *Helmholtz Institute Mainz, Johann-Joachim-Becher-Weg 45, D-55099 Mainz, Germany*
[14] *Henan Normal University, Xinxiang 453007, People's Republic of China*
[15] *Henan University of Science and Technology, Luoyang 471003, People's Republic of China*
[16] *Huangshan College, Huangshan 245000, People's Republic of China*
[17] *Hunan University, Changsha 410082, People's Republic of China*
[18] *Indiana University, Bloomington, Indiana 47405, USA*

[19] (A)INFN Laboratori Nazionali di Frascati, I-00044, Frascati, Italy; (B)INFN and University of Perugia, I-06100, Perugia, Italy
[20] Johannes Gutenberg University of Mainz, Johann-Joachim-Becher-Weg 45, D-55099 Mainz, Germany
[21] Joint Institute for Nuclear Research, 141980 Dubna, Moscow region, Russia
[22] KVI, University of Groningen, NL-9747 AA Groningen, The Netherlands
[23] Lanzhou University, Lanzhou 730000, People's Republic of China
[24] Liaoning University, Shenyang 110036, People's Republic of China
[25] Nanjing Normal University, Nanjing 210023, People's Republic of China
[26] Nanjing University, Nanjing 210093, People's Republic of China
[27] Nankai university, Tianjin 300071, People's Republic of China
[28] Peking University, Beijing 100871, People's Republic of China
[29] Seoul National University, Seoul, 151-747 Korea
[30] Shandong University, Jinan 250100, People's Republic of China
[31] Shanxi University, Taiyuan 030006, People's Republic of China
[32] Sichuan University, Chengdu 610064, People's Republic of China
[33] Soochow University, Suzhou 215006, People's Republic of China
[34] Sun Yat-Sen University, Guangzhou 510275, People's Republic of China
[35] Tsinghua University, Beijing 100084, People's Republic of China
[36] (A)Ankara University, Dogol Caddesi, 06100 Tandogan, Ankara, Turkey; (B)Dogus University, 34722 Istanbul, Turkey; (C)Uludag University, 16059 Bursa, Turkey
[37] Universitaet Giessen, D-35392 Giessen, Germany
[38] University of Chinese Academy of Sciences, Beijing 100049, People's Republic of China
[39] University of Hawaii, Honolulu, Hawaii 96822, USA
[40] University of Minnesota, Minneapolis, Minnesota 55455, USA
[41] University of Rochester, Rochester, New York 14627, USA
[42] University of Science and Technology of China, Hefei 230026, People's Republic of China
[43] University of South China, Hengyang 421001, People's Republic of China
[44] University of the Punjab, Lahore-54590, Pakistan
[45] (A)University of Turin, I-10125, Turin, Italy; (B)University of Eastern Piedmont, I-15121, Alessandria, Italy; (C)INFN, I-10125, Turin, Italy
[46] Uppsala University, Box 516, SE-75120 Uppsala
[47] Wuhan University, Wuhan 430072, People's Republic of China
[48] Zhejiang University, Hangzhou 310027, People's Republic of China
[49] Zhengzhou University, Zhengzhou 450001, People's Republic of China

[a] Also at the Novosibirsk State University, Novosibirsk, 630090, Russia
[b] Also at the Moscow Institute of Physics and Technology, Moscow 141700, Russia
[c] Also at University of Texas at Dallas, Richardson, Texas 75083, USA
[d] Also at the PNPI, Gatchina 188300, Russia

Based on a sample of $(225.3 \pm 2.8) \times 10^6$ J/ψ events collected with the BESIII detector, the electromagnetic Dalitz decays of $J/\psi \to Pe^+e^-(P = \eta'/\eta/\pi^0)$ are studied. By reconstructing the pseudoscalar mesons in various decay modes, the decays $J/\psi \to \eta' e^+e^-$, $J/\psi \to \eta e^+e^-$ and $J/\psi \to \pi^0 e^+e^-$ are observed for the first time. The branching fractions are determined to be $\mathcal{B}(J/\psi \to \eta' e^+e^-) = (5.81 \pm 0.16 \pm 0.31) \times 10^{-5}$, $\mathcal{B}(J/\psi \to \eta e^+e^-) = (1.16 \pm 0.07 \pm 0.06) \times 10^{-5}$, and $\mathcal{B}(J/\psi \to \pi^0 e^+e^-) = (7.56 \pm 1.32 \pm 0.50) \times 10^{-7}$, where the first errors are statistical and the second ones systematic.

PACS numbers: 13.20.Gd, 13.40.Gp,14.40.Pq, 13.40.Hq

I. INTRODUCTION

The study of electromagnetic (EM) decays of hadronic states plays an important role in revealing the structure of hadrons and the mechanism of the interactions between photons and hadrons [1]. Notably, the EM Dalitz decays $V \to Pe^+e^-$ of unflavored vector (V) mesons ($V = \rho$, ω, ϕ or J/ψ) are of interest for probing the EM structure arising at the vertex of the transition from vector to pseudoscalar (P) states. In these decays, the lepton pair can be formed by internal conversion of an intermediate virtual photon with invariant-mass $M_{e^+e^-}$. Assuming point-like particles, the variation of the decay rate with $M_{e^+e^-}$ is exactly described by quantum electrodynamics (QED) [2]. For physical mesons, however, the rate will be modified by the dynamic transition form factor $|F_{VP}(q^2)|^2$, where q is the total four-momentum of the lepton pair and $q^2 = M^2_{e^+e^-}$ is their invariant-mass squared. The general form for the q^2-dependent differential decay width for $V \to Pe^+e^-$, normalized to the width of the corresponding radiative decay $V \to P\gamma$, is given by [1]

$$\frac{d\Gamma(V\to Pe^+e^-)}{dq^2\Gamma(V\to P\gamma)} = \frac{\alpha_{em}}{3\pi}|F_{VP}(q^2)|^2\frac{1}{q^2}\left(1-\frac{4m_e^2}{q^2}\right)^{1/2}\left(1+\frac{2m_e^2}{q^2}\right)\left[\left(1+\frac{q^2}{m_V^2-m_P^2}\right)^2-\frac{4m_V^2q^2}{(m_V^2-m_P^2)^2}\right]^{3/2}$$
$$= |F_{VP}(q^2)|^2\times[\mathrm{QED}(q^2)], \quad (1)$$

where m_V is the mass of the initial vector state, m_P and m_e are the masses of the final states pseudoscalar meson and lepton, respectively; α_{em} is the fine structure constant, and $[\mathrm{QED}(q^2)]$ represents the point-like QED result. The magnitude of the form factor can be estimated based on phenomenological models of nonperturbative quantum chromodynamics (QCD) [3–7]. For example, in the vector meson dominance (VMD) model [8], the form factor is governed mainly by the resonance interaction between photons and hadrons in the time-like region. Experimentally, the form factor is directly accessible by comparing the measured invariant-mass spectrum of the lepton pairs from Dalitz decays with the point-like QED prediction [2]. In the simple pole approximation [9, 10] the q^2-dependent form factor is parameterized by

$$|F_{VP}(q^2)| = \frac{1}{(1-q^2/\Lambda^2)}, \quad (2)$$

where the parameter Λ is the spectroscopic pole mass.

The EM Dalitz decays of the light unflavored mesons ρ,ω and ϕ have been intensively studied by the CMD2, SND, NA60 and KLOE experiments [11–15]. For the decays of $\phi\to\eta e^+e^-$ and $\omega\to\pi^0e^+e^-$, the branching fractions and slopes of the form factors Λ^{-2} are measured [12–15] and the results are in agreement with VMD predictions. Recently, however, a measurement of $\omega\to\pi^0\mu^+\mu^-$ from the NA60 experiment [14] obtains a value of Λ^{-2} which is ten standard deviations from the expectations of VMD.

These theoretical and experimental investigations of the EM Dalitz decays of the light vector mesons motivate us to study the rare charmonium decays $J/\psi\to Pe^+e^-$, which should provide useful information on the interaction of the charmonium states with the electromagnetic field. At present, there is no experimental information on these decays. In Ref. [16], by assuming a simple pole approximation, the decay rates are estimated to be 10^{-5} and 10^{-7} for the $J/\psi\to\eta'(\eta)e^+e^-$ and $\pi^0e^+e^-$, respectively. In this paper, we present measurements of the branching fractions of $J/\psi\to Pe^+e^-$. This analysis is based on $(225.3\pm2.8)\times10^6$ J/ψ events [17], accumulated with the Beijing Spectrometer III (BESIII) detector [18], at the Beijing Electron Positron Collider II (BEPCII).

II. THE BESIII EXPERIMENT AND MONTE CARLO SIMULATION

The BESIII detector and BEPCII accelerator represent major upgrades over the previous versions, BESII and BEPC; the facility is used for studies of hadron spectroscopy and τ-charm physics. The design peak luminosity of the double-ring e^+e^- collider, BEPCII, is 10^{33} cm^{-2} s^{-1} at a beam current of 0.93 A. The BESIII detector has a geometrical acceptance of 93% of 4π solid angle and consists of four main components; the inner three are enclosed in a superconducting solenoidal magnet of 1.0 T magnetic field. First, a small-celled, helium-based main drift chamber (MDC) with 43 layers provides charged particle tracking and measurements of ionization energy loss (dE/dx). The average single wire resolution is 135 μm, and the momentum resolution for 1 GeV/c charged particles is 0.5%. Next is a time-of-flight system (TOF) for particle identification (PID) composed of a barrel part made of two layers with 88 pieces of 5 cm thick, 2.4 m long plastic scintillators in each layer, and two end caps with 96 fan-shaped, 5 cm thick, plastic scintillators in each end cap. The time resolution is 80 ps in the barrel, and 110 ps in the end caps, corresponding to a 2σ K/π separation for momenta up to about 1.0 GeV/c. Third is an electromagnetic calorimeter (EMC) made of 6240 CsI (Tl) crystals arranged in a cylindrical shape (barrel) plus two end caps. For 1.0 GeV photons, the energy resolution is 2.5% in the barrel and 5% in the end caps, and the position resolution is 6 mm in the barrel and 9 mm in the end caps. Finally, a muon chamber system made of 1272 m^2 of resistive plate chambers arranged in 9 layers in the barrel and 8 layers in the end caps is incorporated in the return iron of the superconducting magnet. The position resolution is about 2 cm.

Optimization of event selection and estimations of physical backgrounds are performed using Monte Carlo (MC) simulated samples. The GEANT4-based [19] simulation software BOOST includes the geometric and material descriptions of the BESIII detector, the detector response and digitization models, and also tracks the detector running conditions and performance. The production of the J/ψ resonance is simulated by the MC event generator KKMC [20]; the known decay modes are generated by EVTGEN [21, 22] with branching ratios set at the world average values [23], while unknown decays are generated by LUNDCHARM [24]. The analysis is performed in the framework of the BESIII offline software system which takes care of the detector calibration, event reconstruction and data persistency.

In this analysis, $J/\psi\to\eta'e^+e^-$ is studied using $\eta'\to\gamma\pi^+\pi^-$ and $\eta'\to\pi^+\pi^-\eta$ with $\eta\to\gamma\gamma$; $J/\psi\to\eta e^+e^-$ is studied using $\eta\to\gamma\gamma$ and $\eta\to\pi^+\pi^-\pi^0$ with $\pi^0\to\gamma\gamma$; $J/\psi\to\pi^0e^+e^-$ is studied using $\pi^0\to\gamma\gamma$. An independent data sample of approximately 2.9 fb^{-1} taken at $\sqrt{s}$=3.773 GeV is utilized to study potential continuum background.

The EVTGEN package is used to generate $J/\psi \to \eta' e^+e^-$, ηe^+e^- and $\pi^0 e^+e^-$ events, with angular distributions simulated according to the amplitude squared in Eq.(3) of Ref. [16]. A simple pole approximation is assumed for the form factor. The decay $\eta \to \pi^+\pi^-\pi^0$ is generated according to the Dalitz plot distribution measured in Ref. [25]. For the decay $\eta' \to \gamma\pi^+\pi^-$, the generator takes ρ-ω interference and box anomaly into account [26], while the decay $\eta' \to \pi^+\pi^-\eta$ is generated with phase space.

III. DATA ANALYSIS

Charged tracks in the BESIII detectors are reconstructed from ionization signals in the MDC. To select well-measured tracks we require the polar angle to satisfy $|\cos\theta| < 0.93$ and that tracks to pass within 10 cm of the interaction point in the beam direction and within 1 cm in the plane perpendicular to the beam. The number of such tracks and their net charge must exactly correspond to the particular final state under study. For particle identification, information from dE/dx and TOF is combined to calculate the probabilities, $\mathrm{Prob_{PID}(i)}$, that these measurements are consistent with the hypothesis that a track is an electron, pion, or kaon; $i = e, \pi, K$ labels the particle type. For both electron and positron candidates, we require $\mathrm{Prob_{PID}(e)} > \mathrm{Prob_{PID}}(\pi)$ and $\mathrm{Prob_{PID}(e)} > \mathrm{Prob_{PID}(K)}$. The remaining tracks are assumed to be pions, without PID requirements.

Electromagnetic showers are reconstructed from clusters of energy depositions in the EMC crystals. The energy deposited in nearby TOF counters is included to improve the reconstruction efficiency and energy resolution. The shower energies are required to be greater than 25 MeV for the barrel region ($|\cos(\theta)| < 0.80$) and 50 MeV for the end cap region ($0.86 < |\cos(\theta)| < 0.92$). The showers in the angular range between the barrel and end cap are poorly reconstructed and excluded from the analysis. To exclude showers from charged particles, a photon candidate must be separated by at least 10° from any charged track. Cluster timing requirements are used to suppress electronic noise and energy depositions unrelated to the event.

Events with the decay modes shown in Table I are selected. Every particle in the final state must be explicitly found. For each mode, a vertex fit is performed on the charged tracks; a loose χ^2 cut ensures that they are consistent with originating from the interaction point. In η'/η channels with $\eta' \to \pi^+\pi^-\eta$ and $\eta \to \pi^+\pi^-\pi^0$, photon pairs are used to reconstruct η or π^0 candidates if the invariant-mass satisfies $m_{\gamma\gamma} \in (480, 600)$ MeV/c^2 or (100, 160) MeV/c^2, respectively. To improve resolution and reduce backgrounds, a four-constraint (4C) energy-momentum conserving kinematic fit is performed. For states with extra photon candidates, the combination with the least $\chi^2_{\rm 4C}$ is selected, and in all cases $\chi^2_{\rm 4C}$ is required to be less than 100.

Table I. For each decay mode, the number of observed signal events (N_S), the number of expected total peaking background events (N_B) in the signal region, and the MC efficiency (ϵ) for signal are given. The uncertainty on N_S is statistical only, and the signal regions are defined to be within 3σ of the nominal pseudoscalar masses.

Modes	N_S	N_B	ϵ
$J/\psi \to \eta' e^+e^-(\eta' \to \gamma\pi^+\pi^-)$	983.3 ± 33.0	27.4 ± 1.0	24.8%
$J/\psi \to \eta' e^+e^-(\eta' \to \pi^+\pi^-\eta)$	373.0 ± 19.9	8.5 ± 0.3	17.6%
$J/\psi \to \eta e^+e^-(\eta \to \pi^+\pi^-\pi^0)$	84.2 ± 9.6	5.3 ± 0.3	14.9%
$J/\psi \to \eta e^+e^-(\eta \to \gamma\gamma)$	235.5 ± 16.4	8.7 ± 0.3	22.7%
$J/\psi \to \pi^0 e^+e^-(\pi^0 \to \gamma\gamma)$	39.4 ± 6.9	1.1 ± 0.1	23.4%

Table II. The normalized number of peaking background events ($N_{\gamma-\rm conv}$) from $J/\psi \to P\gamma$ with the photon subsequently converted into an electron-positron pair, and the corresponding MC efficiency ($\epsilon_{\gamma-\rm conv}$) for each background mode.

Mode	$N_{\gamma-\rm conv}$	$\epsilon_{\gamma-\rm conv}$
$J/\psi \to \eta'\gamma(\eta' \to \gamma\pi^+\pi^-)$	25.0 ± 0.9	7.4×10^{-5}
$J/\psi \to \eta'\gamma(\eta' \to \pi^+\pi^-\eta)$	7.6 ± 0.3	3.9×10^{-5}
$J/\psi \to \eta\gamma(\eta \to \pi^+\pi^-\pi^0)$	2.1 ± 0.1	3.7×10^{-5}
$J/\psi \to \eta\gamma(\eta \to \gamma\gamma)$	8.4 ± 0.3	8.6×10^{-5}
$J/\psi \to \pi^0\gamma(\pi^0 \to \gamma\gamma)$	0.7 ± 0.1	8.8×10^{-5}

In the analysis, one of the most important backgrounds comes from events of the radiative decay $J/\psi \to P\gamma$ followed by a γ conversion in the material in front of the MDC, including the beam pipe and the inner wall of the MDC. To suppress these backgrounds, a photon-conversion finder [27] was developed to reconstruct the photon-conversion point in the material. The distance from this reconstructed conversion point to the origin in the x-y plane, defined as $\delta_{xy} = \sqrt{R_x^2 + R_y^2}$, is used to distinguish photon conversion background from signal; R_x and R_y are the distances projected in the x and y directions, respectively. A scatter plot of R_y versus R_x is shown in Fig. 1(a) for the MC simulated decay $J/\psi \to \eta'\gamma(\eta' \to \gamma\pi^+\pi^-)$, in which one of the photons undergoes conversion to an e^+e^- pair. As indicated in Fig. 1(a), the inner circle matches the position of the beam pipe while the outer circle corresponds to the position of the inner wall of the MDC. Figure 1(b) shows the δ_{xy} distributions for the MC simulated $J/\psi \to \eta' e^+e^-$ and $\eta'\gamma$ events, as well as the selected events in the data for comparison. In the δ_{xy} distributions, the two peaks above 2.0 cm correspond to the photon-conversion of the γ from $J/\psi \to \eta'\gamma$ events in the material of the beam pipe and inner wall of the MDC, while the events near $\delta_{xy} = 0$ cm are from the EM Dalitz de-

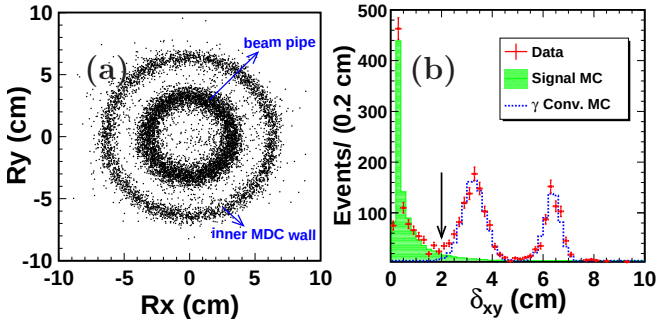

Figure 1. Veto of γ-conversion events. (a) a scatter plot of R_y versus R_x for the MC-simulated $J/\psi \to \eta'\gamma$ ($\eta' \to \gamma\pi^+\pi^-$) events. (b) δ_{xy} distributions. The (green) shaded histogram shows the MC-simulated $J/\psi \to e^+e^-\eta'$ ($\eta' \to \gamma\pi^+\pi^-$) signal events. The (red) dots with error bars are data. The (blue) dotted histogram shows the background from the γ-conversion events. In (b), the solid arrow indicates the requirement on δ_{xy}.

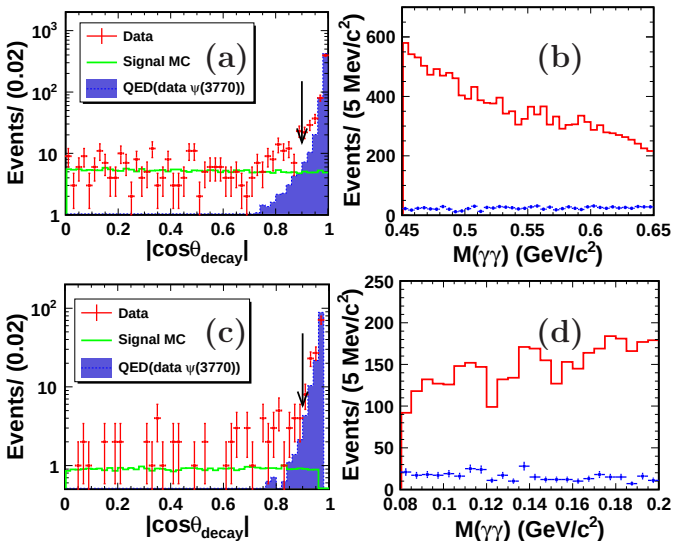

Figure 2. The $|\cos\theta_{\rm decay}|$ distributions (a) for η and (c) for π^0, and two-photon invariant-mass distributions (b) for the $J/\psi \to \eta e^+e^-(\eta \to \gamma\gamma)$ and (d) for the $J/\psi \to \pi^0 e^+e^-(\pi^0 \to \gamma\gamma)$ modes. In (a) and(c), the (green) solid histograms are the MC-simulated signals, the (red) dots with error bars are data, the (blue) dotted histograms are from the $\psi(3770)$ data. The arrows indicate the requirement $|\cos\theta_{\rm decay}| < 0.9$. In (b) and (d), the (red) histograms and the (blue) dots with error bars are $\psi(3770)$ data (used as a continuum sample) without and with the requirement, respectively.

cay. The selected events from data are in good agreement with the MC simulations as shown in Fig. 1(b). Thus we require $\delta_{xy} < 2$ cm to suppress the photon-conversion backgrounds for all signal modes. This requirement retains about 80% of the signal events and removes about 98% of the photon-conversion events from the decay $J/\psi \to \eta'\gamma$. The ability of this requirement to veto the photon-conversion events is the same for the other decay modes. The normalized number of the peaking background events from $J/\psi \to P\gamma$ and the corresponding selection efficiencies are listed in Table II.

In addition to $J/\psi \to P\gamma$, further peaking backgrounds arise from $J/\psi \to \phi P$, ωP and ρP ($P = \eta'$, η or π^0) where ϕ, ω and ρ decay into e^+e^-. Studies based on MC simulations predict 2.2 ± 0.4, 0.8 ± 0.1, 2.8 ± 0.3 and 0.4 ± 0.1 background events for $J/\psi \to \eta' e^+e^-(\eta' \to \gamma\pi^+\pi^-)$, $J/\psi \to \eta' e^+e^-(\eta' \to \pi^+\pi^-\eta)$, $J/\psi \to \eta e^+e^-(\eta \to \pi^+\pi^-\pi^0)$ and $J/\psi \to \pi^0 e^+e^-(\pi^0 \to \gamma\gamma)$ modes, respectively.

Peaking background may also come from $J/\psi \to \pi^+\pi^- P$ with two pions misidentified as an e^+e^- pair. The predicted background levels are 0.2, 0.1, 0.4, and 0.3 events (with negligible errors) for $J/\psi \to \eta' e^+e^-(\eta' \to \gamma\pi^+\pi^-)$, $J/\psi \to \eta' e^+e^-(\eta' \to \pi^+\pi^-\eta)$, $J/\psi \to \eta e^+e^-(\eta \to \pi^+\pi^-\pi^0)$, and $J/\psi \to \eta e^+e^-(\eta \to \gamma\gamma)$, respectively. For $J/\psi \to \pi^0 e^+e^-(\pi^0 \to \gamma\gamma)$, the potential peaking background from $J/\psi \to \pi^+\pi^-\pi^0$ (which has a large branching fraction of $(2.07 \pm 0.12)\%$ [23]) is rejected by requiring $M_{e^+e^-} \leq 0.4$ GeV/c^2. About 80% of signal events are retained and the remaining background is negligible. Background from $J/\psi \to \phi P$ ($\phi \to K^+K^-$) with two kaons misidentified as an e^+e^- pair is also negligible based on the MC simulation. The total expected peaking backgrounds from all sources are summarized in Table I.

For the $J/\psi \to \eta' e^+e^-(\eta' \to \gamma\pi^+\pi^-)$ and $J/\psi \to \eta e^+e^-(\eta \to \pi^+\pi^-\pi^0)$ modes, there are non-peaking backgrounds mainly coming from two sources. One is from $J/\psi \to \gamma\pi^+\pi^-\pi^+\pi^-$ and $J/\psi \to \pi^0\pi^+\pi^-\pi^+\pi^-$. With two pions misidentified as an electron-positron pair, this produces a smooth background under the η' or η mass. The other contribution is from $J/\psi \to \pi^+\pi^-\eta$, $\eta \to \gamma e^+e^-$ and $J/\psi \to \pi^+\pi^-\pi^0$, $\pi^0 \to \gamma e^+e^-$ with the same final states as the signal mode $J/\psi \to \eta' e^+e^-(\eta' \to \gamma\pi^+\pi^-)$. The combined decay rate of $J/\psi \to \pi^+\pi^-\eta$, $\eta \to \gamma e^+e^-$ is at the rate of 10^{-6}; the net contribution is negligible according to the MC simulations. In order to reject background from $J/\psi \to \pi^+\pi^-\pi^0(\pi^0 \to \gamma e^+e^-)$, we veto candidates with an invariant γe^+e^- mass in the interval $[0.10, 0.16]$ GeV/c^2; the remaining background contributes a smooth shape under the η' mass.

For the $J/\psi \to \eta e^+e^-(\eta \to \gamma\gamma)$ and $J/\psi \to \pi^0 e^+e^-(\pi^0 \to \gamma\gamma)$ modes, non-peaking continuum backgrounds from the QED processes $e^+e^- \to e^+e^-\gamma(\gamma)$ and $e^+e^- \to 3\gamma$ (in which one γ converts into an e^+e^- pair) are studied. Since η and π^0 mesons decay isotropically, the angular distribution of photons from η or π^0 decays is flat in $\theta_{\rm decay}$, the angle of the decay photon in the η or π^0 helicity frame. However, continuum background events accumulate near $\cos\theta_{\rm decay} = \pm 1$, and thus we require $|\cos\theta_{\rm decay}| < 0.9$. Figures 2 (a) and (c) show the $|\cos\theta_{\rm decay}|$ distributions for η and π^0 decays, respectively. The (blue) dotted histogram peaking near $|\cos\theta_{\rm decay}| = 1$ in Fig. 2(a) or (c) is from a 2.9 fb^{-1} $\psi(3770)$ data sample taken at $\sqrt{s} = 3.773$ GeV, which is dominated by QED processes. The MC events of $e^+e^- \to e^+e^-\gamma(\gamma)$

and $e^+e^- \to 3\gamma$ are generated using the Babayaga QED event generator [28] and the distributions are consistent with that from the 3.773 GeV sample. After requiring $|\cos\theta_{\rm decay}| < 0.9$, as shown in Fig. 2(b) or (d), the background from QED processes is reduced drastically.

Mass spectra of the signal modes with all of the selection criteria applied are presented in Fig. 3. The signal efficiencies determined from MC simulations for the η', η and π^0 are shown in Table I.

An unbinned extended maximum likelihood (ML) fit is performed for each mode to determine the event yield. The signal probability density function (PDF) in each mode is represented by the signal MC shape convoluted with a Gaussian function, with parameters determined from the fit to the data. The Gaussian function is to describe the MC-data difference due to resolution. The shape for the non-peaking background is described by a first- or second-order Chebychev polynomial, and the background yield and its PDF parameters are allowed to float in the fit. The dominant peaking background from the γ-conversion events in the $J/\psi \to P\gamma$ decay is obtained from the MC-simulated shape with the number fixed to the normalized value. The fitting ranges for the η', η and π^0 modes are $0.85 - 1.05$ GeV/c^2, $0.45 - 0.65$ GeV/c^2 and $0.08 - 0.20$ GeV/c^2, respectively. As discussed in Section III, the estimated numbers of peaking background events are subtracted from the fitted yields. The net signal yields for all modes are summarized in Table I.

To further demonstrate the high quality of signal events, the candidate events within $\pm 3\sigma$ of the pseudoscalar meson mass region for each mode are projected to the $M_{e^+e^-}$ mass distribution in the region of $[0.0, 0.1]$ GeV/c^2 as shown in Fig. 4. The signal MC events are generated based on the amplitude squared in Eq.(3) of Ref. [16] for each mode, normalized to the fitted yield. The number of the peaking backgrounds from γ-conversion events is fixed to the expected value, and the non-peaking backgrounds are estimated by using the sidebands of the pseudoscalar mass spectra. The consistency of the data shapes with signal MC events indicates clear signals in all modes for the EM Dalitz decays $J/\psi \to Pe^+e^-$.

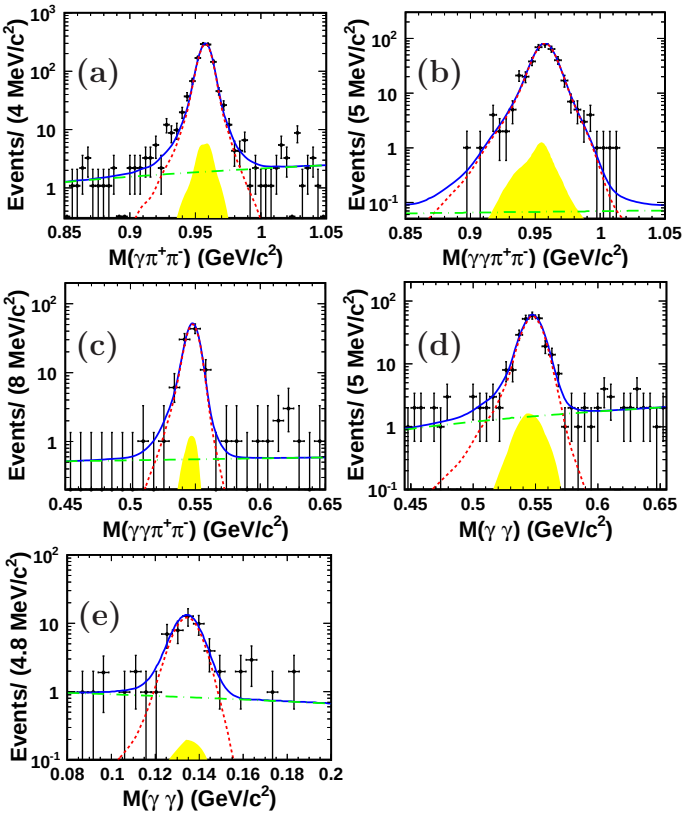

Figure 3. Mass distributions of the pseudoscalar meson candidates in $J/\psi \to Pe^+e^-$: (a) $\eta' \to \gamma\pi^+\pi^-$, (b) $\eta' \to \pi^+\pi^-\eta$ ($\eta \to \gamma\gamma$), (c) $\eta \to \pi^+\pi^-\pi^0$, (d) $\eta \to \gamma\gamma$, and (e) $\pi^0 \to \gamma\gamma$. The (black) dots with error bars are data, the (red) dashed lines represent the signal, the (green) dot-dashed curves shows the non-peaking background shapes, the (yellow) shaded components are the shapes of the peaking backgrounds from the $J/\psi \to P\gamma$ decays. Total fits are shown as the (blue) solid lines.

IV. SYSTEMATIC UNCERTAINTIES

Table III compiles all sources of systematic uncertainties in the measurement of the branching fractions. Most systematic uncertainties are determined from comparisons of clean, high statistics test samples with results from MC simulations.

The MDC tracking efficiency of the charged pion is studied using the control samples of $\psi' \to \pi^+\pi^- J/\psi$, $J/\psi \to l^+l^-$ ($l = e$, μ) and $J/\psi \to \pi^+\pi^-\pi^0$ [29]. The difference between data and MC simulation is 1.0% for each charged pion. The tracking efficiency for the electron or positron is obtained with the control sample of radiative Bhabha scattering $e^+e^- \to \gamma e^+e^-$ (including $J/\psi \to \gamma e^+e^-$) at the J/ψ energy point. The tracking efficiency is calculated with $\epsilon_{\rm electron} = N_{\rm full}/N_{\rm all}$, where $N_{\rm full}$ indicates the number of γe^+e^- events with all final tracks reconstructed successfully; and $N_{\rm all}$ indicates the number of events with one or both charged lepton particles successfully reconstructed in addition to the radiative photon. The difference in tracking efficiency between data and MC simulation is calculated bin-by-bin over the distribution of transverse momentum versus the polar angle of the lepton tracks. The uncertainty is determined to be 1.0% per electron. Tracking uncertainties are treated as fully correlated and thus added linearly.

The photon detection efficiency and its uncertainty are studied using three different methods described in Ref. [29]. On average, the efficiency difference between data and MC simulation is less than 1.0% per photon [29]. The uncertainty from π^0 reconstruction is determined to be 1.0% per π^0 from the control sample $J/\psi \to \pi^+\pi^-\pi^0$ [30], and that for η reconstruction is 1.0% from the control sample $J/\psi \to p\bar{p}\eta$ [30].

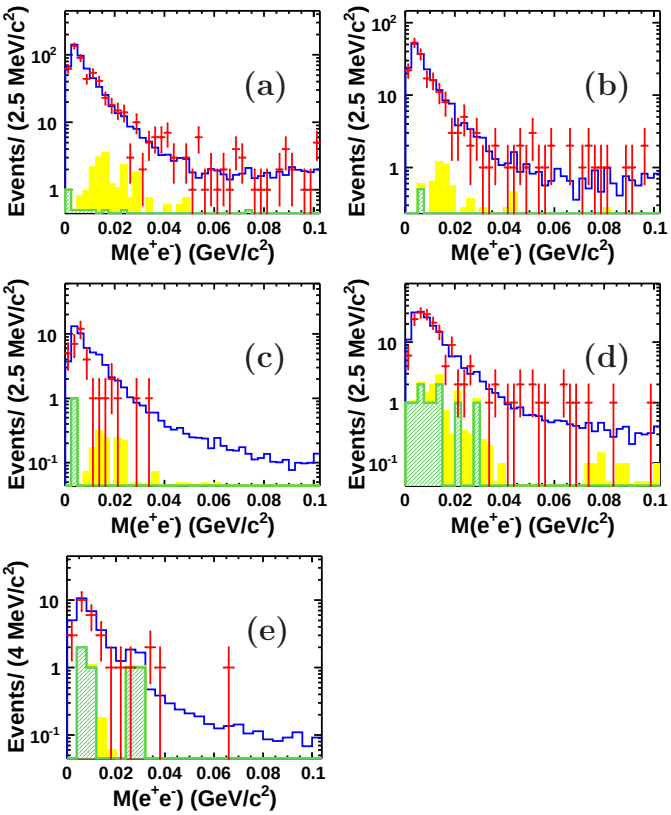

Figure 4. The $M_{e^+e^-}$ mass distributions in $J/\psi \to Pe^+e^-$: (a) $\eta' \to \gamma\pi^+\pi^-$, (b) $\eta' \to \pi^+\pi^-\eta$ ($\eta \to \gamma\gamma$), (c) $\eta \to \pi^+\pi^-\pi^0$, (d) $\eta \to \gamma\gamma$, and (e) $\pi^0 \to \gamma\gamma$. The (red) dots with error bars are data, the (yellow) shaded components are from the γ-conversion backgrounds in the $J/\psi \to P\gamma$ decays, the (green) light-shaded histograms are from non-peaking backgrounds estimated from the sidebands on the pseudoscalar mass spectra. The (blue) histograms represent the sum of backgrounds and MC-simulated signals.

The uncertainty on electron identification is studied with the control sample of radiative Bhabha scattering $e^+e^- \to \gamma e^+e^-$ (including $J/\psi \to \gamma e^+e^-$); samples with backgrounds less than 1.0% are obtained [31]. The efficiency difference for electron identification between the data and MC simulation of about 1.0% is taken as our uncertainty.

In this analysis, the peaking background from the γ-conversion events in $J/\psi \to P\gamma$ decay is suppressed by requiring $\delta_{xy} < 2$ cm. The uncertainty due to this requirement is studied using a sample of $J/\psi \to \pi^+\pi^-\pi^0, \pi^0 \to \gamma e^+e^-$, which includes both the π^0 Dalitz decay and $\pi^0 \to \gamma\gamma$ decay with one of the photons converted to an electron-positron pair. Figures 5 (a) and (c) show the π^0 mass distributions without and with the requirement, and the purity of the sample is better than 99%. The mass distributions of the electron-positron pair are shown in Figs. 5 (b) and (d) for the events without and with the requirement of $\delta_{xy} < 2.0$ cm, respectively. For comparison, the shape of the MC-generated signal is also plotted.

To generate signal events, for the decay $\pi^0 \to \gamma e^+e^-$, the form-factor is modeled by the simple pole approximation as:

$$|F(q^2)| = 1 + \alpha q^2/m^2_{\pi^0}, \quad (3)$$

where q is the total four-momentum of the electron-positron pair, m_{π^0} is the nominal π^0 mass, and $\alpha = 0.032 \pm 0.004$ is the slope parameter [23]. Extended ML fits to the $M_{e^+e^-}$ distributions are performed to obtain the signal yields of the $J/\psi \to \pi^+\pi^-\pi^0(\pi^0 \to \gamma e^+e^-)$ events as shown in Figs. 5 (b) and (d). The data-MC difference of 1.0% is considered as the systematic uncertainty for our γ-conversion veto requiring $\delta_{xy} < 2.0$ cm.

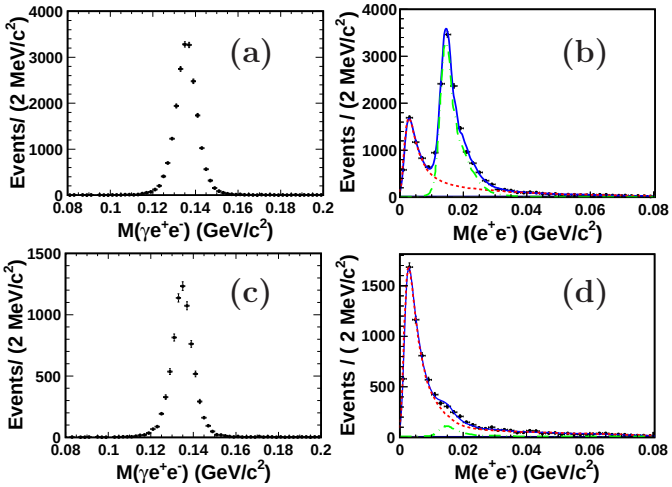

Figure 5. Data of $J/\psi \to \pi^+\pi^-\pi^0, \pi^0 \to \gamma e^+e^-$. The distributions of π^0 masses in (a) and (c); The distributions of the $M_{e^+e^-}$ in (b) and (d). The upper two plots [(a) and (b)] are for events without the requirement of $\delta_{xy} < 2$ cm; the lower two plots [(c) and (d)] are for events with the requirement. The dots with error bars are data. In (b) and (d), the (red) dashed curves are the MC-simulated signals, the (green) dot-dashed curves are the MC-simulated shapes from $J/\psi \to \pi^+\pi^-\pi^0(\gamma\gamma)$ in which one of the photons converts to an electron-positron pair. Total fits are shown as the (blue) solid lines.

The uncertainty from the kinematic fit comes from the inconsistency between the data and MC simulation of the track helix parameters; inaccuracies in our MC simulation of photons have previously been shown to be much smaller [32]. Following the procedure described in Refs. [32, 33], we take the difference between the efficiencies with and without helix parameter corrections as the systematic uncertainty, which is 1.0% in each mode.

In the analysis, the form factor is parameterized by the simple pole approximation as shown in Eq.(2) with the pole mass $\Lambda = m_{\psi'} = 3.686$ GeV/c^2 in the signal MC generator. Direct information on the pole mass is obtained by studying the efficiency-corrected signal yields for each given $M_{e^+e^-}$ bin i for the decay $J/\psi \to \eta' e^+e^-(\eta' \to \gamma\pi^+\pi^-)$, which is the channel with the highest statistics in this analysis. The resolution in

Table III. Summary of systematic uncertainties (%). The terms with asterisks are correlated systematic uncertainties between $\eta' \to \gamma\pi^+\pi^-$ and $\eta' \to \pi^+\pi^-\eta$ ($\eta \to \pi^+\pi^-\pi^0$ and $\eta \to \gamma\gamma$).

	$\eta' \to \gamma\pi^+\pi^-$	$\eta' \to \pi^+\pi^-\eta$	$\eta \to \pi^+\pi^-\pi^0$	$\eta \to \gamma\gamma$	$\pi^0 \to \gamma\gamma$
MDC tracking*	4.0	4.0	4.0	2.0	2.0
Photon detection *	1.0	2.0	2.0	2.0	2.0
$\pi^0(\eta)$ reconstruction	–	1.0	1.0	1.0	1.0
Electron identification*	2.0	2.0	2.0	2.0	2.0
Veto of the γ-conversion*	1.0	1.0	1.0	1.0	1.0
4C kinematic fit	1.0	1.0	1.0	1.0	1.0
Form factor	1.0	1.1	1.1	2.2	3.1
Signal shape	0.9	0.5	0.8	0.1	1.0
Background shape	0.9	1.0	1.0	2.7	4.0
Cited branching fractions	2.0	1.7	1.2	0.5	0.0
Number of J/ψ*	1.2	1.2	1.2	1.2	1.2
Total	5.6	5.8	5.7	5.4	6.6

$M_{e^+e^-}$ is found to be about 5 MeV in the MC simulation. This is much smaller than a statistically reasonable bin width, chosen as 0.1 GeV/c^2, and hence no unfolding is necessary. The signal yields are background subtracted bin-by-bin and then efficiency corrected. By using Eq. (1), the value of the $|F_{J/\psi\eta'}|^2$ is extracted for each given bin i as shown in Fig. 6. Fitting this extracted $|F_{J/\psi\eta'}|^2$ vs. $M_{e^+e^-}$ data, the pole mass in Eq.(2) is determined to be $\Lambda = (3.1 \pm 1.0)$ GeV/c^2. To estimate the uncertainty on the signal efficiency originating from the choice of the pole mass, the signal events are generated with $\Lambda = 3.0$ GeV/c^2 and $\Lambda = 4.0$ GeV/c^2 for each signal mode, respectively. The relative difference of the detection efficiency in each signal mode is taken as the systematic uncertainty, as listed in Table III.

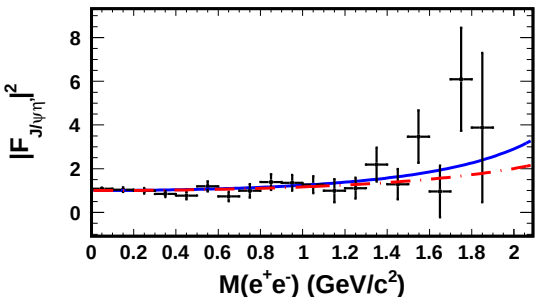

Figure 6. Form factor for $J/\psi \to \eta' e^+e^-(\eta' \to \gamma\pi^+\pi^-)$. The crosses are data, the (red) dot-dashed curve is the prediction of the simple pole model with the pole mass $\Lambda = m_{\psi'} = 3.686$ GeV/c^2, and the fit is shown as the (blue) solid curve.

In the fits to the mass distributions of the pseudoscalar mesons, the signal shapes are described by the MC signal shape convoluted with a Gaussian function. Alternative fits are performed by fixing the signal shape to the MC simulation, and the systematic uncertainties are set based on the changes observed in the yields. The uncertainty due to the non-peaking background shape is estimated by varying the PDF shape and fitting range in the ML fit for each mode. The changes in yields for these variations give systematic uncertainties due to these backgrounds. The numbers of the expected peaking backgrounds from the photon-conversion in radiative decay $J/\psi \to P\gamma$ are summarized in Table II; the errors are negligible for each mode.

The branching fractions for the decay of π^0, η and η' are taken from the world averages [23]. The corresponding uncertainties on the branching fractions are taken as the systematic uncertainties. The uncertainty in the number of J/ψ decays in our data sample is 1.24% [17], which is taken as a systematic uncertainty.

Assuming all systematic uncertainties in Table III are independent, the total systematic uncertainty is obtained by adding them in quadrature. Totals for the five modes range from 5.4% to 6.6%.

V. RESULTS

The branching fractions of the EM Dalitz decays $J/\psi \to Pe^+e^-$, where P stands for η', η and π^0, are calculated with the following formula:

$$\mathcal{B}(J/\psi \to Pe^+e^-) = \frac{N_S}{N_{J/\psi} \cdot \mathcal{B}(P \to F) \cdot \epsilon} \qquad (4)$$

where N_S and ϵ are the number of signal events and the detection efficiency for each mode, respectively, listed in Table I. Here, $N_{J/\psi} = (225.3 \pm 2.8) \times 10^6$ is the number of J/ψ events, and $\mathcal{B}(P \to F)$ is the product of the

Table IV. Summary of the measurements of the branching fractions, where the first uncertainties are statistical and the second ones are systematic. The theoretical prediction [16] for the branching fractions are listed in the last column.

Mode	Branching fraction	Combined Result	Theoretical prediction
$J/\psi \to \eta' e^+e^-(\eta' \to \gamma\pi^+\pi^-)$	$(6.01 \pm 0.20 \pm 0.34) \times 10^{-5}$		
$J/\psi \to \eta' e^+e^-(\eta' \to \pi^+\pi^-\eta)$	$(5.51 \pm 0.29 \pm 0.32) \times 10^{-5}$	$(5.81 \pm 0.16 \pm 0.31) \times 10^{-5}$	$(5.66 \pm 0.16) \times 10^{-5}$
$J/\psi \to \eta e^+e^-(\eta \to \pi^+\pi^-\pi^0)$	$(1.12 \pm 0.13 \pm 0.06) \times 10^{-5}$		
$J/\psi \to \eta e^+e^-(\eta \to \gamma\gamma)$	$(1.17 \pm 0.08 \pm 0.06) \times 10^{-5}$	$(1.16 \pm 0.07 \pm 0.06) \times 10^{-5}$	$(1.21 \pm 0.04) \times 10^{-5}$
$J/\psi \to \pi^0 e^+e^-(\pi^0 \to \gamma\gamma)$	$(7.56 \pm 1.32 \pm 0.50) \times 10^{-7}$	$(7.56 \pm 1.32 \pm 0.50) \times 10^{-7}$	$(3.89^{+0.37}_{-0.33}) \times 10^{-7}$

branching fraction of the pseudoscalar decays into the final states F, taken from the PDG [23]. The calculated branching fractions are summarized in Table IV.

The branching fractions of $J/\psi \to \eta' e^+e^-$ and $J/\psi \to \eta e^+e^-$ measured in different decay modes are consistent with each other within the statistical and uncorrelated systematic uncertainties. In Table III, the items with asterisks denote the correlated systematic errors while the others uncorrelated. The measurements from different modes are therefore combined with the approach in Ref. [34], which uses a standard weighted least-squares procedure taking into consideration the correlations between the measurements. For $J/\psi \to \eta' e^+e^-$, the correlation coefficient between $\eta' \to \gamma\pi^+\pi^-$ and $\eta' \to \pi^+\pi^-\eta$ is $\rho(1,2) = 0.46$; for $J/\psi \to \eta e^+e^-$, it is $\rho(1,2) = 0.13$. The weighted averages of the BESIII measurements are listed in Table IV.

VI. SUMMARY

In summary, with a sample of $(225.3 \pm 2.8) \times 10^6$ J/ψ events in the BESIII detector, the EM Dalitz decays $J/\psi \to Pe^+e^-$, where P stands for η', η and π^0, have been observed for the first time. The branching fractions of $J/\psi \to \eta' e^+e^-$, $J/\psi \to \eta e^+e^-$ and $J/\psi \to \pi^0 e^+e^-$ are measured to be: $\mathcal{B}(J/\psi \to \eta' e^+e^-) = (5.81 \pm 0.16 \pm 0.31) \times 10^{-5}$, $\mathcal{B}(J/\psi \to \eta e^+e^-) = (1.16 \pm 0.07 \pm 0.06) \times 10^{-5}$ and $\mathcal{B}(J/\psi \to \pi^0 e^+e^-) = (7.56 \pm 1.32 \pm 0.50) \times 10^{-7}$, respectively. The measurements for $J/\psi \to \eta' e^+e^-$ and $J/\psi \to \eta e^+e^-$ decay modes are consistent with the theoretical prediction in Ref. [16]. However, the theoretical prediction for the decay rate of $J/\psi \to \pi^0 e^+e^-$ based on the VMD model is $(3.89^{+0.37}_{-0.33}) \times 10^{-7}$, about 2.5 standard deviations from the measurement in this analysis, which may indicate that further improvements of the QCD radiative and relativistic corrections are needed.

VII. ACKNOWLEDGMENT

The BESIII collaboration thanks the staff of BEPCII and the computing center for their strong support. The authors thank Mao-Zhi Yang for useful discussions. This work is supported in part by the Ministry of Science and Technology of China under Contract No. 2009CB825200; Joint Funds of the National Natural Science Foundation of China under Contracts Nos. 11079008, 11179007, 11179014, U1332201; National Natural Science Foundation of China (NSFC) under Contracts Nos. 10625524, 10821063, 10825524, 10835001, 10935007, 11125525, 11235011; the Chinese Academy of Sciences (CAS) Large-Scale Scientific Facility Program; CAS under Contracts Nos. KJCX2-YW-N29, KJCX2-YW-N45; 100 Talents Program of CAS; German Research Foundation DFG under Contract No. Collaborative Research Center CRC-1044; Istituto Nazionale di Fisica Nucleare, Italy; Ministry of Development of Turkey under Contract No. DPT2006K-120470; U. S. Department of Energy under Contracts Nos. DE-FG02-04ER41291, DE-FG02-05ER41374, DE-FG02-94ER40823, DESC0010118; U.S. National Science Foundation; University of Groningen (RuG) and the Helmholtzzentrum fuer Schwerionenforschung GmbH (GSI), Darmstadt; WCU Program of National Research Foundation of Korea under Contract No. R32-2008-000-10155-0.

[1] L. G. Landsberg, Phys. Rept. **128**, 301 (1985).
[2] N. M. Kroll and W. Wada, Phys. Rev. **98**, 1355 (1955).
[3] N. N. Achasov and A. A. Kozhevnikov, Sov. J. Nucl. Phys. **55**, 449 (1992) [Yad. Fiz. **55**, 809 (1992)].
[4] C. Terschlusen and S. Leupold, Phys. Lett. B **691**, 191 (2010).
[5] A. Faessler, C. Fuchs and M. I. Krivoruchenko, Phys. Rev. C **61**, 035206 (2000).
[6] F. Klingl, N. Kaiser and W. Weise, Z. Phys. A **356**, 193 (1996).
[7] G. Kopp, Phys. Rev. D **10**, 932 (1974).

[8] V. M. Budnev and V. A. Karnakov, Pisma Zh. Eksp. Teor. Fiz. **29**, 439 (1979).

[9] D. Becirevic and A. B. Kaidalov, Phys. Lett. B **478**, 417 (2000).

[10] T. Becher and R. J. Hill, Phys. Lett. B **633**, 61 (2006).

[11] R. R. Akhmetshin *et al.* (CMD-2 Collaboration), Phys. Lett. B **613**, 29 (2005).

[12] R. R. Akhmetshin *et al.* (CMD-2 Collaboration), Phys. Lett. B **501**, 191 (2001); Phys. Lett. B **503**, 237 (2001).

[13] M. N. Achasov *et al.* (SND Collaboration), Phys. Lett. B **504**, 275 (2001).

[14] R. Arnaldi *et al.* (NA60 Collaboration), Phys. Lett. B **677**, 260 (2009).

[15] C. Di Donato, AIP Conf. Proc. **1322**, 152 (2010).

[16] J. Fu, H. B. Li, X. Qin and M. Z. Yang, Mod. Phys. Lett. A **27**, 1250223 (2012).

[17] M. Ablikim *et al.* (BESIII Collaboration), Chin. Phys. C **36**, 915 (2012).

[18] M. Ablikim *et al.* (BESIII Collaboration), Nucl. Instrum. Meth. A **614**, 345 (2010).

[19] S. Agostinelli *et al.* (GEANT4 Collaboration), Nucl. Instrum. Meth. A **506**, 250 (2003).

[20] S. Jadach, B. F. L. Ward, and Z. Was, Comput. Phys. Commun.**130**, 260 (2000); Phys. Rev. D **63**, 113009 (2001).

[21] D. J. Lange, Nucl. Instrum. Methods Phys. Res., Sect. A **462**, 152 (2001).

[22] R. -G. Ping, Chin. Phys. C **32**, 599 (2008).

[23] J. Beringer *et al.* (Particle Data Group), Phys. Rev. D **86**, 010001 (2012).

[24] J. C. Chen, G. S. Huang, X. R. Qi, D. H. Zhang and Y. S. Zhu, Phys. Rev. D **62**, 034003 (2000).

[25] J. G. Layter, J. A. Appel, A. Kotlewski, W. Lee, S. Stein, and J. J. Thaler, Phys. Rev. D **7**, 2565 (1973).

[26] M. Ablikim *et al.* (BESIII Collaboration), Phys. Rev. D **87**, 092011 (2013).

[27] Z. R. Xu and K. L. He, Chinese Phys. C **36**, 742 (2012).

[28] C. M. Carloni Calame, G. Montagna, O. Nicrosini, and F. Piccinini, Nucl. Phys. B, Proc. Suppl. **131**, 48 (2004), and references therein.

[29] M. Ablikim *et al.* (BESIII Collaboration), Phys. Rev. D **83**, 112005 (2011).

[30] M. Ablikim *et al.* (BESIII Collaboration), Phys. Rev. D **81**, 052005 (2010).

[31] M. Ablikim *et al.* (BESIII Collaboration), Phys. Rev. D **87**, 032006 (2013).

[32] M. Ablikim *et al.* (BESIII Collaboration), Phys. Rev. D **87**, 012002 (2013).

[33] M. Ablikim *et al.* (BESIII Collaboration), Phys. Rev. D **86**, 092008 (2012).

[34] G. D'Agostini, Nucl. Instrum. Meth. A **346**, 306 (1994).